Inorg. Chem. **2000,** *39,* 3978−3987

An Integrated Approach to the Mid-Spin State ($S = 3/2$) in Six-Coordinate Iron(III) Chiroporphyrins

Jean-Pierre Simonato,[‡] Jacques Pécaut,[‡] Laurent Le Pape,[‡] Jean-Louis Oddou,[‡] Claudine Jeandey,[‡] Maoyu Shang,[§] W. Robert Scheidt,*[,§] Jacek Wojaczyński,[||] Stanisław Wołowiec,[||,⊥] Lechosław Latos-Grażyński,*[,||] and Jean-Claude Marchon*[,‡]

Laboratoire de Chimie de Coordination, Service de Chimie Inorganique et Biologique, Département de
Recherche Fondamentale sur la Matière Condensée, CEA-Grenoble, 38054 Grenoble, France,
Department of Chemistry and Biochemistry, University of Notre Dame, Notre Dame, Indiana 46556,
and Department of Chemistry, University of Wrocław, 14 F. Joliot-Curie Street, Wrocław 50383, Poland

Received February 14, 2000

An intermediate-spin state very close to the mid-spin state ($S = 3/2$) can be stabilized in a ferric porphyrin by an integrated approach which combines the favorable effects of a weak axial field strength and of a small macrocycle hole. Axial ligand exchange by reaction of chloroiron(III)tetramethylchiroporphyrin [(TMCP)FeCl] with silver perchlorate in ethanol−chloroform leads to ethanol-ligated ferric chiroporphyrins. Two distinct crystalline products containing a bisethanol complex [$[(\text{TMCP})\text{Fe}^{\text{III}}(\text{EtOH})_2]\text{ClO}_4$] and three variants of a mixed ethanol−water complex [$[(\text{TMCP})\text{Fe}^{\text{III}}(\text{EtOH})(\text{H}_2\text{O})]\text{ClO}_4$] have been structurally characterized in the solid state. The small hole of the ruffled chiroporphyrin and the weak axial oxygen ligation result in strongly tetragonally distorted complexes. The six-coordinate species exhibit long axial Fe−O bond distances (2.173(5)−2.272(4) Å) and the shortest equatorial Fe−N(av) distances (1.950(5)−1.978(7) Å) found as yet in a ferric porphyrin, reflecting a singly occupied d_{z^2} orbital and a largely depopulated $d_{x^2-y^2}$ orbital. An intriguing case of bond-stretch isomerism is seen for the axial Fe−O bonds in two crystallographically independent mixed ethanol−water species, and it is accounted for by their distinct intra- and intermolecular hydrogen-bond arrays. The Mössbauer spectrum ($\delta = 0.35(1)$ mm s^{-1} and $\Delta E_Q = 3.79(1)$ mm s^{-1} at 77 K) indicates a strong tetragonal distortion around the ferric ion, in agreement with the structural data. The value of the magnetic moment ($\mu_{\text{eff}} = 3.8\ \mu_B$ in the range 50−300 K) strongly supports a mid-spin state ($S = 3/2$). The EPR spectrum at 80 K ($g_\perp \approx 4.0$, $g_\| \approx 2.00$) is consistent with a nearly pure mid-spin state ($^4A_2$) with little rhombic distortion. The ^{1}H NMR spectra in CDCl$_3$−EtOH exhibit upfield-shifted resonances for the pyrrole protons ($\delta \approx -30$ ppm) which are consistent with the depopulated iron $d_{x^2-y^2}$ orbital. Solution equilibria with water and various alcohols, and the spin state of the corresponding species, are discussed on the basis of the NMR data. The bisethanol and ethanol−water species are potential models of unknown hemoprotein ligation states such as Tyr(OH)/Tyr(OH) or Tyr(OH)/H$_2$O that could be obtained by site-directed mutagenesis.

Introduction

The close correspondence between the spin state of iron(III) porphyrins or hemoproteins and their axial ligation state was reviewed in 1981,[1] and magnetostructural correlations have been used as guidelines in the design of new types of ferric tetraphenylporphyrin species during the last two decades. In addition to the classical low-spin state ($S = 1/2$) of ferric complexes with two strong-field axial ligands such as imidazole, and the high-spin state ($S = 5/2$) of complexes with a single moderate-field halide ligand, novel structural types such as six-coordinate high-spin and five-coordinate intermediate-spin iron(III) porphyrins have been synthesized and fully characterized. Crystal field theory indicates that increasing tetragonal distortion in ferric tetraphenylporphyrin (e.g., decreasing axial field strength) leads from low-spin to high-spin states, and that it will eventually stabilize the mid-spin state ($S = 3/2$) when the d_{z^2} orbital is close in energy to the d_{xy}, d_{xz}, and d_{yz} and singly occupied, and the $d_{x^2-y^2}$ is considerably higher in energy and vacant. The weak axial field of a pair of water or ethanol ligands leads to an $S = 5/2$ state,[2,3] while weaker ligands such as perchlorate or hexafluoroantimonate[4,5] induce a quantum mixed-spin state ($S = 3/2, 5/2$) found earlier in the low-pH form of *Chromatium vinosum* ferricytochrome *c*′.[6−8] Many attempts to stabilize the mid-spin state ($S = 3/2$) of ferric tetraphenylporphyrin in six-coordinate complexes with very weak axial ligands (tricyanomethanide,[9] 3-chloropyridine,[10] 3,5-dichloropyridine[11]) have resulted rather in mixed-spin states in which the $d_{x^2-y^2}$

[†] Abbreviations: TMCP, tetramethylchiroporphyrin; OMTPP, octamethyltetraphenylporphyrin; OETPP, octaethyltetraphenylporphyrin.

[‡] CEA-Grenoble.

[§] University of Notre Dame.

[||] University of Wroclaw.

[⊥] Present address: Department of Chemistry, Polytechnical University at Rzeszow, 6 Powstancow Warszawy Street, Rzeszow 35959, Poland.

(1) Scheidt, W. R.; Reed, C. A. *Chem. Rev.* **1981**, *81*, 543−555.

(2) Scheidt, W. R.; Cohen, I. A.; Kastner, M. E. *Biochemistry* **1979**, *18*, 3546−3552.

(3) Scheidt, W. R.; Geiger, D. K.; Lee, Y. J.; Gans, P.; Marchon, J.-C. *Inorg. Chem.* **1992**, *31*, 2660−2663.

(4) Reed, C. A.; Mashiko, T.; Bentley, S. P.; Kastner, M. E.; Scheidt, W. R.; Spartalian, K.; Lang, G. *J. Am. Chem. Soc.* **1979**, *23*, 2948−2958.

(5) Shelly, K.; Bartczak, T.; Scheidt, W. R.; Reed, C. A. *Inorg. Chem.* **1985**, *24*, 4325−4330.

(6) Maltempo, M. M. *Chem. Phys. Lett.* **1979**, *60*, 441−444.

(7) Maltempo, M. M.; Eberhart, M. E. *Chem. Phys. Lett.* **1984**, *108*, 204−208.

(8) La Mar, G. N.; Jackson, J. T.; Dugad, L. B.; Cusanovich, M. A.; Bartsch, R. G. *J. Biol. Chem.* **1990**, *265*, 16173−16180.

(9) Summerville, D. A.; Cohen, I. A.; Hatano, K.; Scheidt, W. R. *Inorg. Chem.* **1978**, *17*, 2906−2910.

10.1021/ic000150a CCC: $19.00

orbital is not completely depopulated. Recently, the concept of a magnetochemical series has been introduced to rank the relative field strengths of anionic axial ligands on the basis of the magnetic spectral features of the mixed-spin states.[12]

As mentioned by earlier investigators,[4,13] the choice between high- and mid-spin states is also governed by the energy separation between the $d_{x^2-y^2}$ and d_{xy} orbitals. Thus, besides decreasing the energy of the d_{z^2}, another potential instrument for stabilizing the pure mid-spin state ($S = 3/2$) is to increase the energy of the $d_{x^2-y^2}$ orbital, i.e., the field strength of the porphyrin ligand. The mixed-spin and nearly pure mid-spin states found for the chloroiron(III) complexes of phthalocyanine[14,15] and tetraazaporphyrin,[16,17] respectively, have been correlated to the stronger interaction of these macrocycles with the iron $d_{x^2-y^2}$ orbital, due to their smaller hole relative to that of the porphyrins. In a similar vein, ferric complexes of sterically crowded porphyrins, which exhibit nonplanar distortions of the macrocycle and consequent contraction of their Fe−N distances, have been investigated very recently. Despite an unusually short Fe−N(av) distance of 2.034(9) Å, the ruffled chiroporphyrin complex FeCl(TMCP) exhibits a high-spin state ($S = 5/2$),[18] while the saddle-shaped FeCl(OMTPP) and FeCl(OETPP) with comparable Fe−N(av) distances (2.034(6) and 2.031(5) Å) have been assigned a mixed-spin state ($S = 3/2, 5/2$) with a 4−40% mid-spin admixture in a high-spin state.[13,19]

These previous attempts suggest that the elusive pure mid-spin state could be stabilized by a synthetic strategy integrating the favorable effects of a weak axial field strength and of a small macrocycle hole in a sterically crowded ferric porphyrin.[20−24] In the present paper we report the structural and magnetic properties of two six-coordinate iron(III) chiroporphyrin species with bisethanol or ethanol−water axial ligation, which exhibit a ground state close to the pure mid-spin state ($S = 3/2$). Finally we discuss the structural features that could lead to the stabilization of a mid-spin ferric state in a hemoprotein.

Experimental Section

Materials. Reagent grade reactants and solvents were used as received from chemical suppliers. Tetramethylchiroporphyrin [H_2(TMCP)] was prepared from 1(*R*)-*cis*-caronaldehyde (biocartol) by previously published methods.[25,26] Iron insertion leading to the high-spin (TMCP)Fe^{III}Cl species (**1**) was carried out as described in a recent publication.[18]

General Spectroscopic Information. UV−vis spectra were recorded on a Perkin-Elmer Lambda 9. Infrared spectra were recorded on a FT-IR Perkin-Elmer 1600 spectrometer. Routine ^{1}H NMR spectra were obtained at ambient temperature on a Bruker AC 200 spectrometer using deuterated chloroform solutions with $CHCl_3$ ($\delta = 7.24$ ppm) as an internal standard. Mass spectra were measured with a ZAB2-SEQ instrument. Elemental analyses were performed by SCA/CNRS, Vernaison, France.

Synthesis of [(TMCP)Fe^{III}(EtOH)$_2$]ClO_4. A 48 mg amount of **1** (5.3×10^{-5} mol) was dissolved in 10 mL of chloroform, and a solution of 15.6 mg of silver perchlorate (1.4 equiv) in 10 mL of ethanol was added. The mixture was warmed to 35 °C for 10 min, the silver chloride precipitate was filtered off over Celite, and the filtrate was brought to dryness on a rotary evaporator. The brown product was taken up in the minimum volume of dichloromethane, and crystallization was induced by addition of hexane. Yield: 50.6 mg of **2** (90%). *Caution! Although we have not encountered any problems, it should be noted that perchlorate salts are potentially explosive. Small quantities should be prepared only and handled with the appropriate care*. MS (FAB$^+$): $m/z = 867.3$, $[M - 2(C_2H_5OH) - ClO_4]^+$. Anal. Found: C, 53.08; H, 5.58; Fe, 4.57. Calcd for $[(TMCP)Fe(EtOH)_2](ClO_4)\cdot(H_2O)_{0.67}(CHCl_3)$: C, 53.41; H, 5.61; Fe, 4.69. UV−vis (CH_2Cl_2): λ_{max} 402 (Soret), 544, 692 nm. ^{1}H NMR ($CDCl_3$): δ −33.8, −36.0 ppm (β-pyrrolic protons of the mixed-ligation species, vide infra). ^{1}H NMR ($CDCl_3-C_2H_5OH$ mixture, 20/1 v/v): δ −30.6, −31.9 ppm (β-pyrrolic protons of the bisethanol complex). The exact nature of the microcrystalline product **2** is discussed below.

X-ray Crystal Structure Determinations. Single crystals suitable for X-ray analysis were obtained by slow diffusion of *n*-hexane in a saturated chloroform solution of **2**, resulting in a crystal lattice (**3**) containing both the bisethanol complex [(TMCP)Fe^{III}(EtOH)$_2$]ClO_4 and the mixed ethanol−water complex [(TMCP)Fe^{III}(EtOH)(H_2O)]ClO_4. Another batch obtained from a chloroform−hexane mixture with a presumably higher content in residual water gave a crystal lattice (**4**) containing only the mixed species.

Dark brown crystals of **3** and **4** were mounted on glass needles. Graphite-monochromated Mo Kα radiation ($\lambda = 0.710\,73$ Å) was used throughout. Crystallographic data are listed in Table 1. Intensity data for **3** were collected at 130(2) K on an Enraf-Nonius FAST area detector diffractometer with our standard methods for small molecules.[27] Intensity data for **4** were collected at 193(2) K on a Bruker SMART CCD detector. Data collection was performed by a hemisphere run taking frames (30 s) at 0.30° in ω. The data were corrected for Lorentz and polarization effects. A semiempirical absorption correction using the programs DIFABS for **3** and SADABS [28] for **4** was carried out. The Bruker ShelXTL[29] software package was used for the solution, refinement, and artwork of the structures. Both structures were solved and refined by direct methods and difference Fourier techniques performed on DEC or Silicon Graphics workstations. Neutral atom scattering factors were used.[30] All non-hydrogen atoms were refined anisotropically. All hydrogen atoms were placed at calculated positions and refined as riding atoms with isotropic displacement parameters.

---

(10) Scheidt, W. R.; Geiger, D. K.; Hayes, R. G.; Lang, G. *J. Am. Chem. Soc.* **1983**, *105*, 2625−2632.

(11) Scheidt, W. R.; Osvath, S. R.; Young, J.; Reed, C. A.; Shaevitz, B.; Gupta, G. P. *Inorg. Chem.* **1989**, *28*, 1591−1595.

(12) Reed, C. A., Guiset, F. *J. Am. Chem. Soc.* **1996**, *118*, 3281−3282.

(13) Cheng, R.-J.; Chen, P.-Y.; Gau, P.-R.; Chen, C.-C.; Peng, S.-M. *J. Am. Chem. Soc.* **1997**, *119*, 2563−2569.

(14) Kennedy, B. J.; Brain, G.; Murray, K. S. *Inorg. Chim. Acta* **1984**, *81*, L29-L31.

(15) Kennedy, B. J.; Murray, K. S.; Zwack, P. R.; Homborg, H.; Kalz, W. *Inorg. Chem.* **1986**, *25*, 2539−2545.

(16) Fitzgerald, J. P.; Haggerty, B. S.; Rheingold, A. L.; May, L. *Inorg. Chem.* **1992**, *31*, 2006−2013.

(17) Fitzgerald, J. P.; Yap, G. P. A.; Rheingold, A. L.; Brewer, C. T.; May, L.; Brewer, G. A. *J. Chem. Soc., Dalton Trans.* **1996**, 1249−1253.

(18) Mazzanti, M.; Marchon, J.-C.; Wojaczynski, J.; Wolowiec, S.; Latos-Grazynski, L.; Shang, M.; Scheidt, W. R. *Inorg. Chem.* **1998**, *37*, 2476−2481.

(19) Schünemann, V.; Gerdan, M.; Trautwein, A. X.; Haoudi, N.; Mandon, D.; Fischer, J.; Weiss, R.; Tabard, A.; Guilard, R. *Angew. Chem., Int. Ed. Engl.* **1999**, *38*, 3181−3183.

(20) The combination of axial chloride ligation and carbene insertion into an Fe^{III}−N bond of tetraphenylporphyrin results in a nearly pure mid-spin state; see refs 21 and 22.

(21) Latos-Grazynski, L.; Cheng, R.-J.; La Mar, G. N.; Balch, A. L. *J. Am. Chem. Soc.* **1981**, *103*, 4270−4272.

(22) Mansuy, D.; Morgenstern-Badarau, I.; Lange, M.; Gans, P. *Inorg. Chem.* **1982**, *21*, 1427−1430.

(23) Weak axial ligation by perchlorate and strongly electron-releasing porphyrin substituents lead to a nearly pure mid-spin state in perchloratoiron(III) tetrakis(2,4,6-trimethoxyphenyl)porphyrin; see ref 24.

(24) Toney, G. E.; terHaar, L. W.; Savrin, J. E.; Gold, A.; Hatfield, W. E.; Sangaiah, R. *Inorg. Chem.* **1984**, *23*, 2561−2563.

(25) Veyrat, M.; Fantin, L.; Desmoulins, S.; Petitjean, A.; Mazzanti, M.; Ramasseul, R.; Marchon, J.-C.; Bau, R. *Bull. Soc. Chim. Fr.* **1997**, *134*, 703−711.

(26) Pérollier, C.; Mazzanti, M.; Simonato, J.-P.; Launay, F.; Ramasseul, R.; Marchon, J.-C. *Eur. J. Org. Chem.* **2000**, 583−589.

(27) Scheidt, W. R.; Turowska-Tyrk, I. *Inorg. Chem.* **1994**, *33*, 1314−1318.

(28) Sheldrick, G. M. (Universität Göttingen), 1994.

(29) Interactive Molecular Graphics, release 5.1, Bruker AXS, Inc., Madison, WI 53719, 1998.

(30) *International Tables for X-ray Crystallography*; Kynoch Press: Birmingham, England.

Table 1. Crystallographic Data for the Ethanol-Ligated Ferric Tetramethylchiroporphyrin Complexes **3** and **4**

	3[a]	**4**[b]		**3**[a]	**4**[b]
empirical formula	$C_{157.45}H_{197.45}N_{12}O_{44}FeCl_{7.35}$	$C_{105}H_{127}N_8O_{29}Fe_2Cl_{17}$	space group	*C*2	*P*1
fw	3390.83	2679.5	*Z*	2	2
cryst syst	monoclinic	triclinic	D_c, Mg/m^3	1.354	1.428
a, Å	47.576(2)	13.1966(2)	wavelength, Å	0.710 73	0.710 73
b, Å	12.9029(15)	13.8900(2)	μ, cm^{-1}	4.58	6.70
c, Å	13.664(2)	17.8102(0)	temp, K	130(2)	193(2)
α, deg		79.215(1)	R1 [$I > 2\sigma(I)$][c]	0.0671	0.0587
β, deg	97.353(4)	76.486(1)	wR2 [$I > 2\sigma(I)$][c]	0.1604	0.1611
γ, deg		89.173(1)	Flack index	0.01(2)	0.02(2)
V, Å^3	8318.6(14)	3116.70(7)			

[a] $[(TMCP)Fe(EtOH)_2](ClO_4)\cdot[(TMCP)Fe(H_2O)(EtOH)]_2(EtOH)_2(ClO_4)_2\cdot(CHCl_3)_{1.45}$. [b] $[(TMCP)Fe(H_2O)(EtOH)](ClO_4)\cdot[(TMCP)Fe(H_2O)(EtOH)](H_2O)(ClO_4)\cdot(CHCl_3)_5$. [c] $R1 = \sum||F_o| - |F_c||/\sum|F_o|$ and $wR2 = \{\sum[w(F_o^2 - F_c^2)^2]/\sum[wF_o^4]\}^{1/2}$. The conventional *R* factors R1 are based on *F*, with *F* set to zero for negative F^2. The criterion of $F^2 < 2\sigma(F^2)$ was used only for calculating R1. *R* factors based on F^2 (wR2) are statistically about twice as large as those based on *F*, and *R* factors based on all data will be even larger.

Magnetization Measurements. The solid-state magnetization of a 19.7 mg sample of **2** (1.9×10^{-5} mol) was measured under helium on a Quantum Design MPMS SQUID magnetometer from 2 to 300 K at a field of 0.5 T. The sample was contained in a Kel-F bucket. The bucket was measured independently at the same field and temperatures. The raw data were corrected for the sample holder contribution, and the molar susceptibility corresponds to the resulting magnetization per mole and per magnetic field unit. The diamagnetic contribution of the sample ($\chi_{dia} = -710 \times 10^{-6}$ cm^3 mol^{-1}) was evaluated using Pascal's constants. The data were fitted with the following equation based on the spin-Hamiltonian $H = \beta\vec{H}\cdot\tilde{g}\cdot.\hat{S} + \hat{S}\cdot\tilde{D}\cdot S$ for $S = 3/2$:

$$\chi T = \alpha\frac{g_{\|}^{2}\left[1 + 9\exp\left(-\frac{2D}{kT}\right)\right] + 8g_{\perp}^{2}\left\{1 + \frac{3kT}{4D}\left[1 - \exp\left(-\frac{2D}{kT}\right)\right]\right\}}{32\left[1 + \exp\left(-\frac{2D}{kT}\right)\right]} + \beta T$$

which is valid for $T > 6$ K and for $|D| \gg g_x\beta H_x = 0.45$ cm^{-1} with $g_x = 2$ and $H_x = 0.5$ T. The α parameter can take into account the uncertainty concerning the exact composition of the microcrystalline sample. The β parameter represents the related diamagnetic component uncertainty, as well as the temperature-independent paramagnetism and the saturated ferromagnetism of impurities.

EPR Spectroscopy. Low-temperature EPR spectra were recorded on an X-band Bruker EMX spectrometer equipped with an Oxford Instruments ESR-900 continuous-flow helium cryostat and a ER-4116 OM Bruker cavity. Magnetic field values were measured with an EMX-035M NMR gaussmeter. Simulated spectra were calculated with a program written by F. Neese (Universität Konstanz, Germany, August 1994).

NMR Spectroscopy. ^{1}H NMR spectra were recorded on a Varian Unity 400 MHz or on a Bruker AMX spectrometer operating in the quadrature mode at 300 MHz. The residual ^{1}H NMR resonances of deuterated solvents were used as a secondary reference. Solution magnetic moments were measured using the Evans method.[31]

Mössbauer Spectroscopy. ^{57}Fe Mössbauer experiments were performed at 77 K and room temperature. The samples were mounted in a conventional horizontal transmission cryostat equipped with a beryllium window. The ^{57}Co(Rh) source was moved in either the constant or sinusoidal acceleration mode at room temperature. The 14.4 keV γ-rays were detected by means of a proportional counter, and Mössbauer spectra were recorded on a 512-channel analyzer working in the multiscanning mode. Spectra were analyzed by least-squares fits using two Lorentzian lines of equal intensities. Isomer shift values are given relative to α-Fe at room temperature.

Results

Synthesis and X-ray Structures of the Ethanol Complexes. As expected from the known chemistry of ferric tetraphenylporphyrin complexes,[3] axial ligand metathesis by reaction of (TMCP)FeCl with silver perchlorate in a 1:1 ethanol−chloroform mixture affords bisethanol-ligated ferric chiroporphyrins (see below). Adventitious water in the solvents used for crystal growth can act as a competitive axial ligand, leading to the isolation of both a bisethanol complex and a mixed ethanol−water complex in the crystalline product, as indicated by the X-ray structures. Crystals of **3** belong to the space group *C*2 of the monoclinic system, and the unit cell contains one $[(TMCP)Fe^{III}(EtOH)_2]ClO_4$ unit (**3a**), with crystallographically required 2-fold symmetry, and two crystallographically equivalent $[(TMCP)Fe^{III}(EtOH)(H_2O)]ClO_4$ species (**3b**), as well as solvent molecules (ethanol, chloroform). Crystals of **4** belong to the space group *P*1 of the triclinic system, and the unit cell contains two crystallographically inequivalent $[(TMCP)Fe^{III}(EtOH)(H_2O)]ClO_4$ species (**4a** and **4b**), as well as solvent molecules (water, chloroform). The bulk product **2** probably contains microcrystalline **3**, and maybe some **4** as well (see the Discussion). The structures of the four cations **3a**,**b** and **4a**,**b** are shown in Figures 1 and 2. Selected bond distances and angles are given in Table 2.

The bisethanol complex **3a** and the three crystallographically distinct ethanol−water complexes **3b**, **4a**, and **4b** share a number of structural features: a ruffled porphyrin core with considerable radial contraction (Fe−N(av) distances 1.950(5)−1.978(7) Å), long axial Fe−O distances (2.173(5)−2.272(4) Å), and an array of intramolecular hydrogen bonds between the hydroxyl groups of the axial ligands and the ester carbonyl groups of the *meso*-cyclopropyl substituents. A ruffled porphyrin core has been found in all the structures of tetramethylchiroporphyrin complexes that have been solved so far.[18,32−37] This type of distortion is required to accommodate the alternating up, down *meso*-cyclopropyl substituents and is thus a consequence of the α, *β*, α, *β* conformation. However, the degree of ruffling and the related average metal−nitrogen distance are dependent on the nature of the complex.[18,32−37] The mixed species **3b**, **4a**, and **4b** exhibit significantly shorter iron−nitrogen bond distances (Fe−N(av) 1.950(5) Å for each) than the bisethanol complex **3a** (Fe−N(av) 1.978(7) Å). Formal diagrams of the porphinato core showing the pattern of displacements of atoms from the 24-atom mean plane for the four cations are given in Figure 3. Also shown in this figure are averaged values of bond distances and angles in the cores. The out-of-plane displacements from the 24-atom macrocyclic core for the *meso* carbon atoms are −0.44 Å for C(m5) and 0.51 Å for C(m6) for the bisethanol complex **3a**; the values are 0.68, −0.69, 0.67, and −0.63 Å for

---

(31) Evans, D. F.; James, T. A. *J. Chem. Soc., Dalton Trans.* **1979**, 723−726.

(32) Mazzanti, M.; Veyrat, M.; Ramasseul, R.; Marchon, J.-C.; Turowska-Tyrk, I.; Shang, M.; Scheidt, W. R. *Inorg. Chem.* **1996**, *35*, 3733−3734.

(33) Toronto, D.; Sarrazin, F.; Pécaut, J.; Marchon, J.-C.; Shang, M.; Scheidt, W. R. *Inorg. Chem.* **1998**, *37*, 526−532.

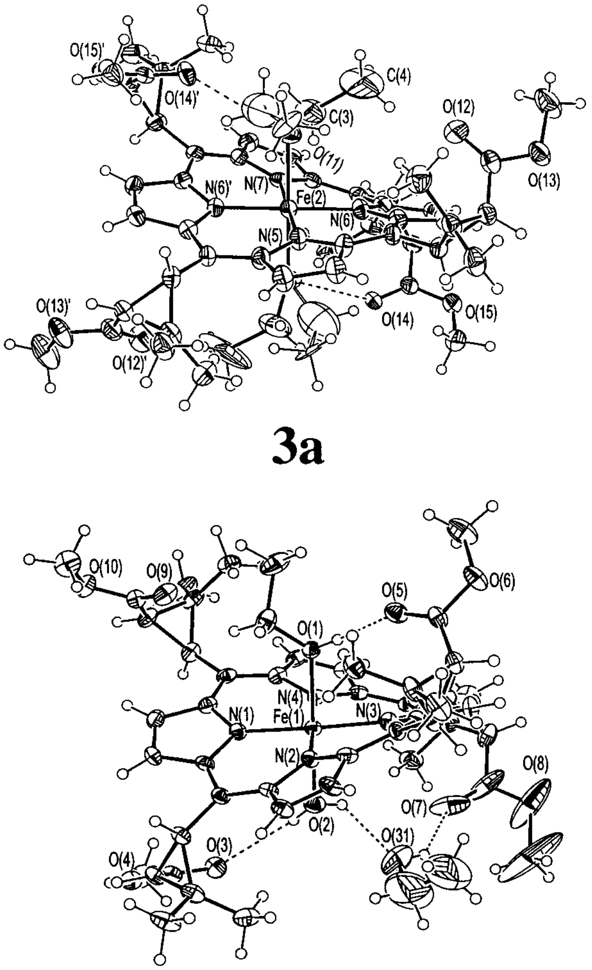

3a

3b

Figure 1. Perspective view and atom labels of the cations [(TMCP)-Fe^{III}(EtOH)$_2$]$^+$ (**3a**) and [(TMCP)Fe^{III}(EtOH)(H$_2$O)](EtOH)$^+$ (**3b**) in crystal **3**.

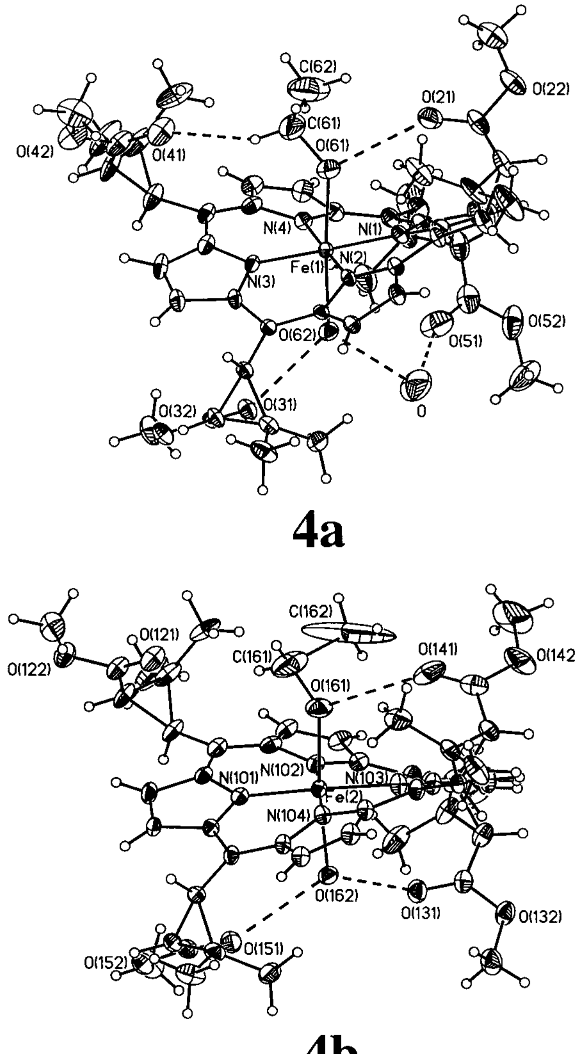

4a

4b

Figure 2. Perspective view and atom labels of the cations [(TMCP)-Fe^{III}(EtOH)(H$_2$O)](H$_2$O)$^+$ (**4a**) and [(TMCP)Fe^{III}(EtOH)(H$_2$O)]$^+$ (**4b**) in crystal **4**.

the mixed species **3b**, and their average values are 0.68, −0.66, 0.58, and −0.64 Å for the two independent mixed species **4a** and **4b**. The angles between adjacent pyrrole rings of the porphyrin are 19.9(3)° and 19.5(2)° for the bisethanol complex **3a**, and 29.2(3)°, 26.3(4)°, 31.9(3)°, and 25.8(3)° for the mixed species **3b**; their average values are 27.4(3)°, 25.5(2)°, 27.2(2)°, and 25.7(2)° for **4a** and **4b**. Thus, the cores of the cations with mixed ethanol−water ligation appear to be substantially more ruffled than that of the bisethanol complex, with consequently shorter Fe−N(av) distances.

The axial ligands of the bisethanol species **3a** are disordered on two symmetry-related sites, while the axial ligands of the mixed water−ethanol species **3b**, **4a**, and **4b** are ordered (Figures 1 and 2). The hydrogen-bond arrays found in the four cations are depicted schematically in Figure 4. In **3a**, there is an intramolecular hydrogen bond between the hydroxyl group and a carbonyl group of a *meso* substituent (O−O distance of O(11)−H···O(14), 3.145(8) Å). Similar intramolecular hydrogen-bonding patterns are observed for the ethanol ligand of the mixed species **3b**, **4a**, and **4b**: hydroxylic H atom to *meso*-carbonyl (O(1)−H···O(5) 2.820(6) Å in **3b**; O(61)−H···O(21) 2.938(6) Å in **4a**, and O(161)−H···O(141) 3.212(7) Å in **4b**). The hydrogen-bond pattern of the axial aqua ligand is different in each of the three structural variants **3b**, **4a**, and **4b**. In **4b** it involves the two *meso*-carbonyl groups as hydrogen bond acceptors (O(162)−H···O(131) 2.958(5) Å and O(162)−H···O(151) 2.974(7) Å). In **4a**, the bonding array of the coordinated water involves a *meso*-carbonyl group (O(62)−H···O(31) 3.022(6) Å) and a second water molecule (O(62)−H···O 2.638(8) Å) as hydrogen bond acceptors; the latter is also hydrogen bonded to O(51) of a *meso*-carbonyl (O−H···O(51) 2.693(9) Å) and to a perchlorate counteranion. The short distance (2.638(8) Å) between the two water molecules indicates a very strong hydrogen bond. A case similar to that of **4a** is seen in the mixed cation **3b**: in addition to the usual interaction with a *meso*-carbonyl (O(2)−H···O(3) 3.076(8) Å), the aqua ligand is involved as a donor in a strong hydrogen bond to O(31) of an interstitial ethanol molecule (O(2)−H···O(31) 2.617(9) Å), which in turn interacts with a *meso*-carbonyl acceptor (O(31)−H···O(7) 2.752(9) Å).

Magnetization Measurements. The magnetization properties of a microcrystalline sample of **2**, with a composition presum-

---

(34) Simonato, J.-P.; Pécaut, J.; Marchon, J.-C. *J. Am. Chem. Soc.* **1998**, *120*, 7363−7364.

(35) Simonato, J.-P.; Pécaut, J.; Scheidt, W. R.; Marchon, J.-C. *Chem. Commun.* **1999**, 989−990.

(36) Pérollier, C.; Pécaut, J.; Ramasseul, R.; Bau, R.; Marchon, J.-C. *Chem. Commun.* **1999**, 1597−1598.

(37) Pérollier, C.; Pécaut, J.; Ramasseul, R.; Marchon, J.-C. *Inorg. Chem.* **1999**, *38*, 3758−3759.

Table 2. Selected Bond Distances (Å) and Angles (deg) for the Ethanol-Ligated Ferric Tetramethylchiroporphyrin Complexes **3** and **4**

3		**4**	
Lengths			
Fe(l)−N(4)	1.944(5)	Fe(1)−N(3)	1.941(3)
Fe(l)−N(l)	1.951(4)	Fe(1)−N(4)	1.945(4)
Fe(l)−N(3)	1.951(5)	Fe(1)−N(1)	1.957(3)
Fe(l)−N(2)	1.953(5)	Fe(1)−N(2)	1.958(3)
Fe(l)−O(2)	2.173(5)	Fe(1)−O(62)	2.195(3)
Fe(l)−O(l)	2.240(4)	Fe(1)−O(61)	2.272(4)
Fe(2)−N(6)′	1.973(5)	Fe(2)−N(104)	1.944(3)
Fe(2)−N(6)	1.973(5)	Fe(2)−N(102)	1.949(3)
Fe(2)−N(7)	1.977(8)	Fe(2)−N(103)	1.953(3)
Fe(2)−N(5)	1.990(10)	Fe(2)−N(101)	1.953(3)
Fe(2)−O(11)′	2.179(5)	Fe(2)−O(161)	2.187(4)
Fe(2)−O(11)	2.179(5)	Fe(2)−O(162)	2.267(3)
Angles			
N(4)−Fe(1)−N(1)	90.0(2)	N(3)−Fe(1)−N(4)	90.55(13)
N(4)−Fe(1)−N(3)	89.9(2)	N(3)−Fe(1)−N(1)	177.61(14)
N(1)−Fe(1)−N(3)	177.3(2)	N(4)−Fe(1)−N(1)	90.69(13)
N(4)−Fe(1)−N(2)	178.4(2)	N(3)−Fe(1)−N(2)	89.51(13)
N(l)−Fe(l)−N(2)	90.2(2)	N(4)−Fe(1)−N(2)	178.66(14)
N(3)−Fe(1)−N(2)	89.8(2)	N(1)−Fe(1)−N(2)	89.20(13)
N(4)−Fe(1)−O(2)	93.3(2)	N(3)−Fe(1)−O(62)	87.30(12)
N(1)−Fe(1)−O(2)	86.9(2)	N(4)−Fe(1)−O(62)	92.64(13)
N(3)−Fe(1)−O(2)	95.8(2)	N(1)−Fe(1)−O(62)	94.68(13)
N(2)−Fe(1)−O(2)	88.3(2)	N(2)−Fe(1)−O(62)	88.71(13)
N(4)−Fe(l)−O(l)	90.2(2)	N(3)−Fe(1)−O(61)	94.61(13)
N(1)−Fe(1)−O(1)	92.9(2)	N(4)−Fe(1)−O(61)	93.36(15)
N(3)−Fe(1)−O(1)	84.4(2)	N(1)−Fe(1)−O(61)	83.29(14)
N(2)−Fe(1)−O(1)	88.1(2)	N(2)−Fe(1)−O(61)	85.30(14)
O(2)−Fe(1)−O(1)	176.5(2)	O(62)−Fe(1)−O(61)	173.69(13)
N(6)′−Fe(2)−N(6)	179.4(4)	N(104)−Fe(2)−N(102)	179.23(15)
N(6)′−Fe(2)−N(7)	89.7(2)	N(104)−Fe(2)−N(103)	89.51(13)
N(6)−Fe(2)−N(7)	89.7(2)	N(102)−Fe(2)−N(103)	90.68(13)
N(6)′−Fe(2)−N(5)	90.3(2)	N(104)−Fe(2)−N(101)	90.27(13)
N(6)−Fe(2)−N(5)	90.3(2)	N(102)−Fe(2)−N(101)	89.51(13)
N(7)−Fe(2)−N(5)	180.000(2)	N(103)−Fe(2)−N(101)	177.84(15)
N(6)′−Fe(2)−O(11)′	94.0(2)	N(104)−Fe(2)−O(161)	87.11(15)
N(6)−Fe(2)−O(11)′	85.9(2)	N(102)−Fe(2)−O(161)	93.64(15)
N(7)−Fe(2)−O(11)′	87.9(2)	N(103)−Fe(2)−O(161)	87.11(14)
N(5)−Fe(2)−O(11)′	92.1(2)	N(101)−Fe(2)−O(161)	95.03(14)
N(6)′−Fe(2)−O(11)	85.9(2)	N(104)−Fe(2)−O(162)	87.40(13)
N(6)−Fe(2)−O(11)	94.0(2)	N(102)−Fe(2)−O(162)	91.86(13)
N(7)−Fe(2)−O(11)	87.9(2)	N(103)−Fe(2)−O(162)	87.43(13)
N(5)−Fe(2)−O(11)	92.1(2)	N(101)−Fe(2)−O(162)	90.41(12)
O(11)′−Fe(2)−O(11)	175.9(3)	O(161)−Fe(2)−O(162)	172.29(13)

ably similar to that of crystal **3** (see the Discussion), have been investigated to evaluate the spin state of the iron centers and their associated zero-field splitting. Figure 5 illustrates the temperature dependence of the product of molar susceptibility by temperature. It shows a plateau at $\chi T \approx 1.84$ cm^3 K mol^{-1} ($\mu_{\mathrm{eff}} = 3.8\ \mu_{\mathrm{B}}$) at high temperatures (300−50 K). This value is close to that expected (1.875 cm^3 K mol^{-1}) for a mid-spin state ($S = 3/2$) following the Curie law. At lower temperatures, χT decreases as can be expected if the complex presents a zero-field splitting component. The possibility of a spin−spin interaction can be ruled out since the minimum distance between adjacent paramagnetic centers is larger than 10 Å. The data were fitted with the equation described in the Experimental Section, in which $g_{\parallel}$ and $g_{\perp}$ were constant ($g_{\parallel} = g_{\perp} = 2$) and D, α, and β were variable parameters. The best fit was obtained with $|D| = 5.8(5)$ cm^{-1}, α = 0.98(2), close to 1 as expected, and $\beta = 2.3(2) \times 10^{-3}$ cm^3 mol^{-1}, and it is shown in Figure 5.

EPR Spectroscopy. The X-band EPR spectrum of a frozen solution of **1** in toluene−dichloromethane (1/1 v/v) is shown in Figure 6A. At 4.2 K this three-line signal is easily saturable, and a microwave power lower than 0.2 mW must be used to obtain an unsaturated spectrum. Broadening of the three lines is observed at temperatures higher than 10 K. At 25 K a single line is observed in the $g_{\perp}$ region. This type of signal with $g_{\perp} \approx 6$ and $g_{\parallel} \approx 2$ is expected for a high-spin ferric porphyrin such as **1**. The simulation of spectrum A shown in Figure 6B was obtained with $g_x = 6.14$, $g_y = 5.79$, and $g_z = 2.001$.

The X-band EPR spectra of a microcrystalline sample of **2**, shown in Figure 7, give further evidence for the presence of a nearly pure mid-spin Fe$^{\mathrm{III}}$ ion. In addition to the signal of **2** (see below), a signal with a maximum at $g_{\perp} = 6$ and a minimum at $g_{\parallel} = 1.98$ is detected only at very low temperatures (4.2 K in Figure 7A) and corresponds to a minor high-spin ferric species. This species, which is not saturated in the experimental conditions of Figure 7A, is distinct from **1** as indicated by this different saturation behavior. At 80 K the main signal is that of **2**, which shows broad components at $g_{\perp} \approx 4$ and $g_{\parallel} \approx 2$ (Figure 7B). A simulation of the latter signal was obtained assuming an effective spin $S' = 1/2$. A set of g values in accordance with the rhombogram for an $S = 3/2$ spin[6] assuming $g_{\mathrm{real}} = 2$ was obtained: $g_y = 4.3$, $g_x = 3.7$, and $g_z = 2.0$ (Figure 7C). These values imply a very small rhombicity of $E/D \approx 0.05$.

Mössbauer Spectroscopy. The zero-field Mössbauer spectra of **2** and of the parent high-spin complex **1** are shown in Figure 8, and Table 3 summarizes the data. The spectrum of microcrystalline **1** at room temperature displays an asymmetric quadrupole doublet which is characteristic of a five-coordinate high-spin iron(III) porphyrin.[38] On the other hand, the very large quadrupole splitting which is observed in the spectra of **2** ($\Delta E_{\mathrm{Q}} = 3.79(1)$ mm s^{-1} at 77 K) is within the range ($\Delta E_{\mathrm{Q}} = 3.0$−4.3 mm s^{-1}) reported for strongly tetragonally distorted five-coordinate iron(III) complexes which exhibit intermediate-spin ground states.[39,40] A weak high-spin ferric species is seen in the spectrum of **2** at 77 K (Figure 8B), and the corresponding signal cannot be fit with the Mössbauer parameters of **1**. This minor species is probably the origin of the $g = 6$ and 1.98 signal seen at 4.2 K in the EPR spectrum of **2** (see above).

^{1}H NMR Spectral Characterization in Solution. The ^{1}H NMR spectrum of **2** in a $CDCl_3$−C_2H_5OH mixture (20/1 v/v) is shown in Figure 9. The resonance assignments have been made on the basis of relative intensities, signal multiplicities, and line width analysis. Signal positions are given in Table 4. The line multiplicities (two pyrrole resonances and one set of *meso* resonances) are consistent with an effective D_2 symmetry in solution, resulting from axial coordination of two ethanol molecules and fast rotation on the NMR time scale around the Fe−O bonds of the $[(\mathrm{TMCP})\mathrm{Fe}(C_2H_5OH)_2]^+$ species. The upfield position of the pyrrole resonances at −30.6 and −31.9 ppm is diagnostic of a largely depopulated iron $d_{x^2-y^2}$ orbital[21,22,41−43] in agreement with the intermediate-spin state found for the solid complex. Addition of an excess of ethanol to a solution of (TMCP)FeCl in $CDCl_3$ led to the same ^{1}H NMR spectrum.

A stepwise conversion of the high-spin (TMCP)FeCl complex to a bismethanol adduct was followed by ^{1}H NMR spectroscopy. Titration of a 5 mM solution of (TMCP)FeCl in $CDCl_3$ at 293 K with CD_3OD induces the gradual growth of a new set of

---

[38] Sams, J. R.; Tsin, T. B. In *The Porphyrins, Vol. IV*; Dolphin, D., Ed.; Academic Press: New York, 1979; pp 425−478.

[39] Kostka, K. L.; Fox, B. G.; Hendrich, M. P.; Collins, T. J.; Rickard, C. E. F.; Wright, L. J.; Münck, E. *J. Am. Chem. Soc.* **1993**, *115*, 6746−6757.

[40] Keutel, H.; Käpplinger, I.; Jäger, E.-G.; Grodzicki, M.; Schünemann, V.; Trautwein, A. X. *Inorg. Chem.* **1999**, *38*, 2320−2327.

[41] La Mar, G. N. Walker, F. A. In *The Porphyrins*; Dolphin, D., Ed.; Academic Press: New York, 1979; p 61.

[42] Bertini, I.; Luchinat, C. *NMR of Paramagnetic Molecules in Biological Systems*; The Benjamin/Cummings Publishing Co.: Reading, MA, 1986.

[43] Walker, F. A.; Simonis, U. In *Biological Magnetic Resonance, Volume 12 NMR of Paramagnetic Molecules*; Berliner, L. J., Reuben, J., Eds.; Plenum Press: New York, 1993; p 133.

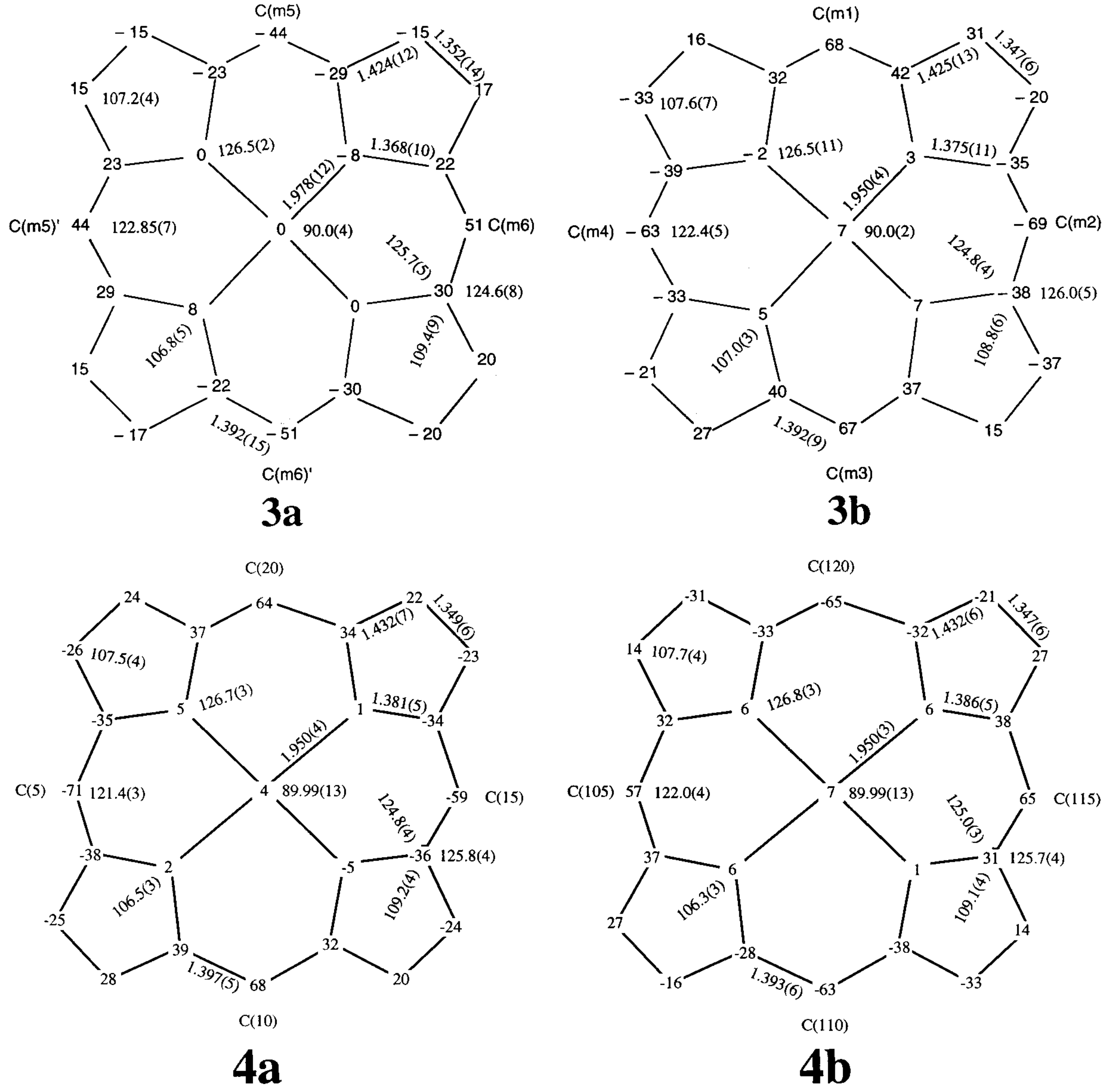

Figure 3. Formal diagrams of the porphinato core showing the patterns of displacements of atoms from the 24-atom mean plane (in units of 0.01 Å) for the cations **3a**, **3b**, **4a**, and **4b**.

resonances, while the intensities of the parent compound resonances decrease as shown in Figure 10. Total conversion to the bismethanol adduct is not achieved even at a 1000:1 molar ratio of CD_3OD to **1** in $CDCl_3$ solution, but the bismethanol adduct was formed quantitatively when (TMCP)FeCl was dissolved in CD_3OD at 298 K. Identical spectra were obtained when (TMCP)FeCl, (TMCP)FeBr, and (TMCP)FeI were dissolved in CD_3OD, confirming that a cationic bisalcohol complex is formed. The spectral pattern of the bismethanol complex resembles that obtained for the bisethanol complex, although noticeable shift differences are seen: for example, at 298 K the two pyrrole resonances of the bismethanol species are superimposed at δ −26.8 ppm, and they are resolved only below 283 K, while at 295 K a resolved pair is observed at −30.6 and −31.9 ppm for the bisethanol complex (Table 4). A magnetic moment of 4.1 ± 0.3 μ_B at 297 K was measured by the Evans method for the $[(TMCP)Fe(CD_3OD)_2]^+$ species obtained by dissolving (TMCP)FeCl in a $CD_3OD-CDCl_3$ mixture (4.3/1 v/v), in good agreement with the value ($\mu_{eff} = 3.8\ \mu_B$) found for **2** in the solid state.

Contrary to methanol and ethanol, the addition of *sec*-butanol to (TMCP)FeCl or (TMCP)FeBr failed to produce an alcohol adduct, even in the presence of 500 equiv of *sec*-butanol at very low temperature (203 K in CD_2Cl_2). However, after substitution of axial chloride by perchlorate by shaking a $CDCl_3$ solution of (TMCP)FeCl with a small amount of silver perchlorate, titration with *sec*-butanol leads to an intermediate-spin spectral pattern attributed to the $[(TMCP)Fe(sec\text{-}C_4H_9OH)_2]^+$ complex (Table 4). Identical spectra were obtained when (*RS*)-*sec*-butanol and (*S*)-*sec*-butanol were used, although the formation of three diastereomeric species is expected in the first case.[33] We presume that the effect of axial ligand chirality on the tertiary carbon atom may be masked by broadening of the resonances due to dynamic effects, such as fast ligand exchange and inversion on oxygen.

Finally, coordination of water on iron(III) tetramethylchiroporphyrin results in effects very similar to those of alcohol ligands. A sample of (TMCP)FeCl dissolved in $CDCl_3$ was shaken with a solution of $AgClO_4$ in D_2O. The putative $[(TMCP)Fe(D_2O)_2]^+$ species produced by axial ligand metathesis exhibited spectral features similar to those of the bisethanol complex, with two upfield-shifted pyrrole resonances at −33.7 and −36.3 ppm (Table 4), indicating an intermediate-spin state. However, the chemical shifts of the protons of the *meso*-

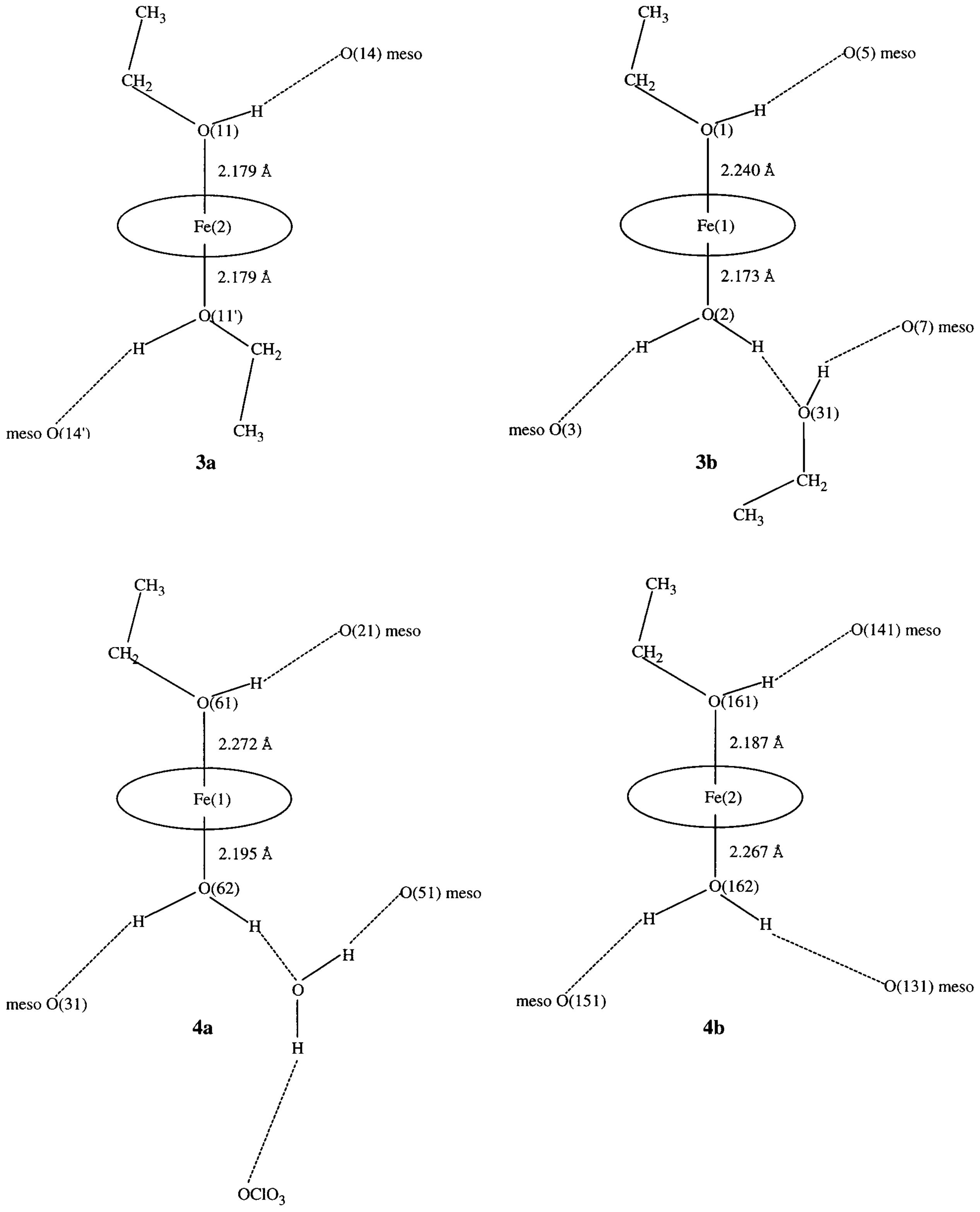

Figure 4. Schematic depiction of the hydrogen-bond arrays in the bisethanol complex **3a** and in the three independent mixed-ligand species **3b**, **4a**, and **4b**, illustrating the bond-stretch isomerism of the Fe—O axial bonds in **4a** and **4b**.

cyclopropyl groups are distinctly different for the pure bisaqua and the pure bisethanol species, and they allow a safe speciation of $[(TMCP)Fe(C_2H_5OH)_2]^+$ in solutions of **2**. In particular, a downfield position of the 1-CH signal (22.8 ppm) is found only for the $[(TMCP)Fe(D_2O)_2]^+$ complex in the series of intermediate-spin complexes investigated.

Discussion

Possible Polymorphism of the Bulk Product 2. It is important to note that the microcrystalline product **2** obtained in the bulk syntheses presumably contains some mixed aqua—ethanol species in addition to the bisethanol complex. Axial ligand exchange between ethanol and adventitious water is fast

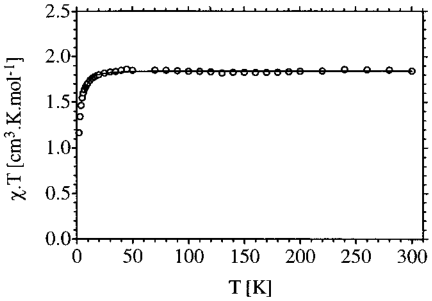

Figure 5. Temperature dependence of the χT product for a microcrystalline sample of **2** in the range 2−300 K (dots), and best least-squares fit to the magnetic data in the range 6−300 K assuming a mid-spin state ($S = 3/2$) (solid line).

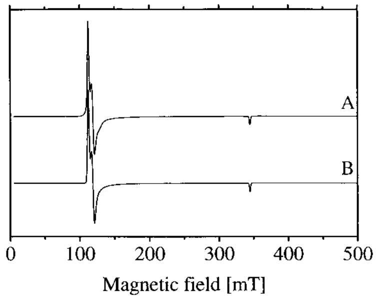

Figure 6. (A) X-band EPR spectra of a frozen solution of (TMCP)-$Fe^{III}Cl$ (**1**), 3.6×10^{-3} mol L^{-1}, in toluene−dichloromethane (1/1 v/v). Experimental conditions: temperature 4.2 K, microwave frequency 9.6558 GHz, microwave power 13 μW, modulation amplitude 10 G, modulation frequency 100 kHz, 1 scan in 336 s. (B) Simulation of spectrum A with $g_x = 6.14$, $g_y = 5.79$, $g_z = 2.001$, $w_x = 13$ G, $w_y = 20$ G, and $w_z = 10$ G.

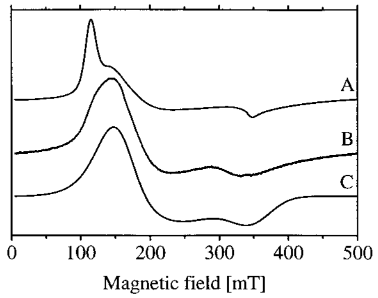

Figure 7. X-band EPR spectra of a microcrystalline sample of **2**. Experimental conditions: (A) temperature 4.2 K, microwave frequency 9.6597 GHz, microwave power 13 mW, modulation amplitude 10 G, modulation frequency 100 kHz, 1 scan in 336 s; (B) temperature 80 K, microwave frequency 9.660 39 GHz, other parameters as for (A); (C) simulation of spectrum B with $g_y = 4.3$, $g_x = 3.7$, $g_z = 2.0$, $w_y = 260$ G, $w_x = 660$ G, and $w_z = 340$ G.

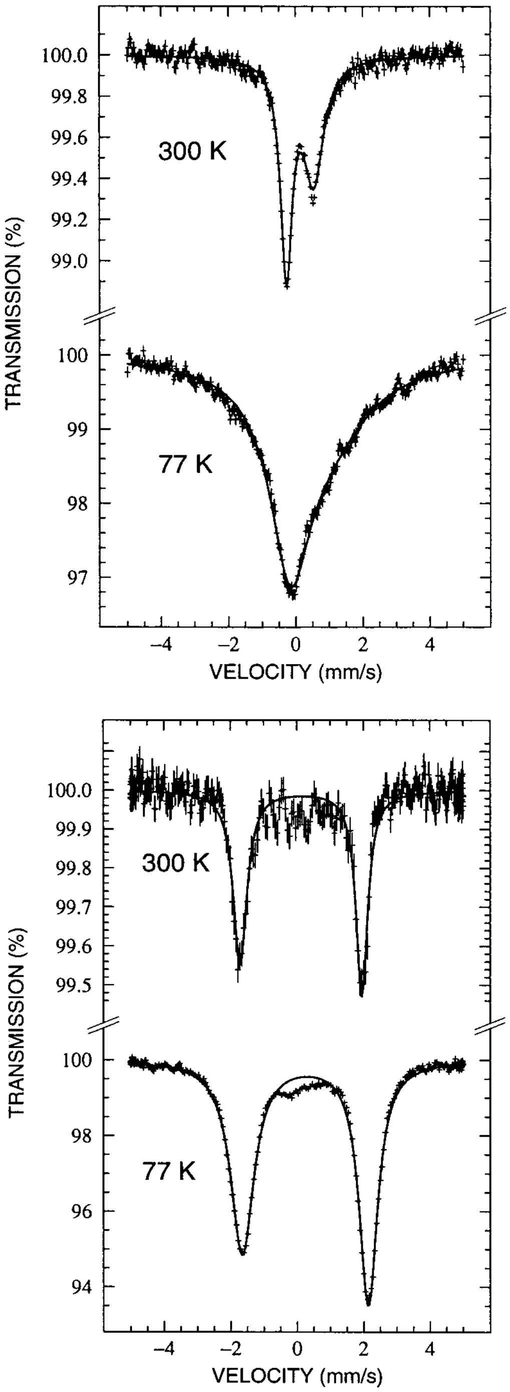

Figure 8. Zero-field Mössbauer spectra of microcrystalline samples of **1** (A, top) and **2** (B, bottom) at 300 and 77 K.

in solution, and crystallization apparently favors the formation of the mixed species even with a considerable excess of ethanol, as suggested by microanalysis and X-ray crystallography. The microanalytical data on **2** indicate the required 2:1 ethanol-to-iron ratio of an authentic bisethanol complex, but they do not provide any structural information. In fact, the microanalysis of **2** is entirely consistent both with a microcrystalline bisethanol complex containing some interstitial water (i.e., formula $[(TMCP)Fe(EtOH)_2](ClO_4)\cdot(H_2O)_{0.67}(CHCl_3))$, and with a composite crystalline product analogous to **3** (i.e., a stoichiometrically equivalent formula such as $[(TMCP)Fe(EtOH)_2][(TMCP)Fe(H_2O)(EtOH)]_2(ClO_4)_3\cdot(EtOH)_2\cdot(CHCl_3)_3)$. The X-ray structures suggest that the crystal lattice of **3**, with its strong hydrogen bonding between the aqua ligand and the interstitial ethanol molecule of **3b**, is presumably more stable than that of a pure bisethanol complex with (or without) interstitial water. Similar considerations also apply to the stable crystal lattice of **4**. Thus, the microcrystalline samples **2** obtained in the bulk syntheses may be polymorphic, and they may contain a mixture of structurally similar species. Examination of **2** with bulk physical probes such as magnetic susceptibility will afford an average measurement for the different species which may be present in the samples. Since these species are structurally very similar, their individual contributions will be difficult to resolve in Mössbauer and EPR spectroscopies. In contrast, the crystal structures of **3** and **4** allow a detailed characterization of each individual species to be performed.

Spin State of Ethanol-Ligated Ferric Chiroporphyrins. Taken together, the short equatorial Fe−N and long axial Fe−O

Table 3. Mössbauer Data of **1** and **2**

	1				**2**			
temp (K)	δ (mm s^{-1})	ΔE_Q (mm s^{-1})	W_1 (mm s^{-1})	W_2 (mm s^{-1})	δ (mm s^{-1})	ΔE_Q (mm s^{-1})	W_1 (mm s^{-1})	W_2 (mm s^{-1})
300	0.25(1)	0.82(1)	0.29(1)	0.60(2)	0.23(1)	3.67(2)	0.37(2)	0.30(2)
77	0.44(2)	1.00(4)	1.30(2)	3.10(8)	0.35(1)	3.79(1)	0.72(1)	0.55(1)

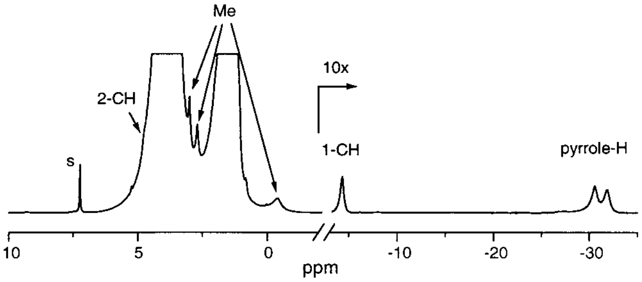

Figure 9. ^{1}H NMR (300 MHz) spectrum of [(TMCP)Fe^{III}(EtOH)$_2$]ClO$_4$ measured in a CDCl$_3$−C$_2$H$_5$OH mixture (20/1 v/v). The upfield part of the spectrum is enlarged 10 times for better presentation.

bonds seen in the structures of **3** and **4** indicate an intermediate-spin state for the bisethanol **3a** and for the mixed ethanol−water **3b**, **4a**, and **4b** species in the solid state. That this state is closer to a mid-spin state ($S = 3/2$) than the previously reported cases of mixed-spin state ($S = 3/2$, $5/2$)[9−13,19] is supported by the values of the bond lengths around the iron(III) center: the average Fe−N bond distances (1.950(5)−1.978(7) Å) are at the shorter end of the range (1.970−2.000 Å) found for low-spin iron(III) porphyrins,[1] and they are indicative of a largely depopulated $d_{x^2-y^2}$ orbital, while the Fe−O distances (2.173(5)−2.272(4) Å) are larger than those (2.095−2.136 Å) found in high-spin iron(III) porphyrins with two ethanol or water ligands,[2,3] and they reflect a singly occupied d_{z^2} orbital.

Consideration of the average iron−nitrogen bond distances in the two species leads to the conclusion that the mixed species is more tetragonally distorted than the bisethanol species: Fe−N(av) = 1.950(5) Å for **3b**, **4a**, and **4b**, while Fe−N(av) = 1.978(7) Å for **3a**. Thus, the $d_{x^2-y^2}$ orbital is probably less depopulated in **3a** than in the mixed species, and the ground state of the latter may be closer to the mid-spin state. The values of the iron−nitrogen bond distances in the two species also reflect their different degrees of ruffling, which may be related to the intramolecular hydrogen-bonding patterns (vide infra). It is also significant that the chemical shifts of the pyrrolic protons in solution reflect the trend seen in the solid state: the resonances of the bisaqua species (−33.7, −36.3 ppm) and those of the species with mixed ligation (−33.8, −36.0 ppm) are more upfield-shifted than those of the pure bisethanol species (−30.6, −31.9 ppm), indicating greater tetragonal distortion in the former.[12]

The large value of ΔE_Q (3.79(1) mm s^{-1} at 77 K) in the Mössbauer spectrum of **2** indicates a considerable tetragonal distortion of the ferric species in the solid state. It is within the range reported for five-coordinate iron(III) complexes which exhibit a mid-spin (3.0−4.3 mm s^{-1})[17,24,39,40] or a mixed-spin (3.5−4.3 mm s^{-1})[12] ground state, and thus it is not diagnostic of the actual spin state ($S = 3/2$, or $S = 3/2$, $5/2$) of the ferric complexes (bisethanol and possibly aqua−ethanol species) which are present in the sample.

Strong evidence for a nearly pure mid-spin state comes from the magnetic susceptibility measurements of **2**: the magnetic moment in the range 50−300 K is close to the spin-only value for a quartet state ($\mu_{\mathrm{eff}} = 3.9\ \mu_B$), and a satisfactory fit of the data can be obtained with a spin Hamiltonian for an $S = 3/2$ state.

A mean measured $g_\perp$ value equal to 4.0 in the EPR spectrum is generally considered as diagnostic of a quartet state ($S = 3/2$), and substantial deviation from this value indicates substantial mixed-spin ($S = 3/2$, $5/2$) character. With the mean simulated $g_\perp$ component at 4.0, the EPR spectrum of **2** indicates a ground state which is a mid-spin state ($S = 3/2$), or very close to a mid-spin state at least. Assuming a pure mid-spin state ($^4A_2$), the calculated values $g_y = 4.3$ and $g_x = 3.7$ imply a small rhombic distortion, $E/D \approx 0.05$.

Structural Consequences of Intramolecular Hydrogen Bonding, and Fe−O Bond-Stretch Isomerism. An intriguing case of bond-stretch isomerism is seen for the axial Fe−O bonds in the two independent mixed species **4a** and **4b**, and it is depicted in Figure 4: the Fe−ethanol distance is larger (2.272(4) Å) than the Fe−water distance (2.195(3) Å) in **4a**, while the opposite situation is seen in **4b**: a long bond (2.267(3) Å) to water and a shorter bond (2.187(4) Å) to ethanol. Consideration of the distinct hydrogen−bonding patterns of the two species provides a plausible explanation for this unusual observation. In **4a** the aqua ligand is a hydrogen-bond donor to a water molecule. The short distance (O···O 2.638(8) Å) between the two water molecules indicates a strong hydrogen bond which presumably enhances the basicity of the aqua ligand. With partial hydroxo character, the latter binds rather strongly to iron, resulting in a short Fe(1)−O(62) bond (2.195(3) Å) and a long Fe(1)−O(61) bond (2.272(4) Å) by the *trans* effect. That is not the case in **4b**, in which the aqua ligand forms only weak hydrogen bonds to the *meso*-carbonyl groups, and is thus a weaker ligand of iron.

A case similar to that of **4a** is seen in the mixed cation **3b**, which displays a long axial bond (2.240(4) Å) to the ethanol ligand and a shorter bond (2.173(5) Å) to the aqua ligand, presumably for the same reason: a strong hydrogen bond from the aqua ligand to the neighboring ethanol molecule (O(2)H···O(31) 2.617(9) Å). It is also interesting to note that the iron−ethanol distances are very similar in **3a** and in **4b**, in which the *trans* ligand is a "normal" water molecule.

The two distinct types of intramolecular hydrogen-bond arrays (with or without an interstitial water or ethanol molecule) may be at the origin of (or related to) the degree of ruffling of the two complexes: a stronger hydrogen bonding may result in a larger degree of ruffling, and thus in a shorter Fe−N(av) distance and in a closer proximity to the pure mid-spin state.

Possible Relevance to Hemoproteins. In principle the combination of nonplanar porphyrin distortion and weak axial ligand field can be found also in hemoproteins, suggesting that a mid-spin state ($S = 3/2$), as yet unknown, could be a biological reality. Highly distorted hemes have been found in a number of hemoprotein crystal structures during the past decade,[44] and water is present as an axial ligand of iron in many proteins such as *met*-aquomyoglobin.[45] Among the amino acids found in proteins, serine, threonine, hydroxylysine, and homoserine have a potentially ligating alcohol group, and tyrosine has a phenol function. Serine has been implicated as a ligand of iron in a

---

[44] Shelnutt, J. A.; Song, X.-Z.; Ma, J.-G.; Jia, S.-L.; Jentzen, W.; Medforth, C. J. *Chem. Soc. Rev.* **1998**, *27*, 31−41.

[45] *Met*-(H$_2$O)Mb: La Mar, G. N.; Budd, D. L.; Smith, K. M.; Langry, K. C. *J. Am. Chem. Soc.* **1980**, *102*, 1822−1827.

Table 4. ^{1}H NMR Data for Mid-Spin Iron(III) Tetramethylchiroporphyrin Complexes [(TMCP)Fe^{III}(ROH)$_2$]X^a

ROH	solvent^b	temp (K)	δ (ppm)			
			pyrrole-H	1-CH	2-CH	CH$_3$
CD_3OD	CD_3OD	298	−26.8	−7.2	∼4.9^c	−0.2, 2.5, 3.2
		283	−28.4, −28.7	−8.2	∼5.1^c	−0.2, 2.5, 3.3
		273	−30.1, −30.6	−9.1	∼5.2^c	−0.2, 2.5, 3.3
		243	−37.6, −38.5	−13.1	∼5.5^c	−0.3, 2.4, 3.6
CD_3OD	$CDCl_3$	297	−32.7, −34.0	−6.1	4.6	−0.4, 2.3, 2.9
C_2H_5OH	$CDCl_3-C_2H_5OH$ (20/1 v/v)	295	−30.6, −31.9	−4.4	∼4.8^c	−0.4, 2.7, 3.0
sec-C_4H_9OH	$CDCl_3-C_4H_9OH$ (20/1 v/v)	295	−29.3, −31.3	d	4.5	−0.4, 2.6, 3.0
D_2O	$CDCl_3-D_2O$	295	−33.7, −36.3	22.8	3.5	−0.8, 2.2, 2.9

^{a} X = Cl for the bis-CD_3OD complex in CD_3OD, and X = ClO_4 for the remaining compounds. ^{b} The positions of the signals are solvent dependent due to a possible ligand exchange and hydrogen bonding. ^{c} Overlapped with a strong solvent signal. ^{d} Not identified.

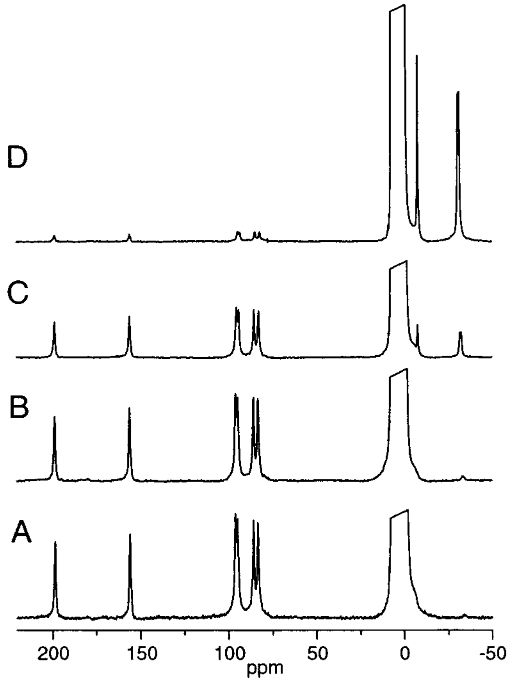

Figure 10. ^{1}H NMR titration of (TMCP)FeCl in $CDCl_3$ with CD_3OD at 293 K. Number of equivalents of CD_3OD added: (A) 50; (B) 100; (C) 300; (D) 1000.

Cys(42)Ser rubredoxin mutant.[46] Axial ligation by tyrosine has been found in several wild-type or mutant proteins.[47−51] Cytochrome *f* has been shown to have His/Tyr ligation, but the donor is the α-amino rather than the phenol group of Tyr1.[48,49] Mutant myoglobins obtained by site-directed mutagenesis, such as His(E7)Tyr or His(F8)Tyr, exhibit tyrosinate rather than tyrosine ligation,[50] as does heme d_1 of cytochrome cd_1.[51] The axial ligand *trans* to thiolate in cytochrome P-450 LM2 has been characterized as tyrosine in an undefined protonation state.[47] Altogether, these results suggest that weak axial ligation of iron(III) of the type Tyr(OH)/Tyr(OH) or Tyr(OH)/H_2O, if it exists at all, is probably rare in wild-type hemoproteins. However, site-directed mutagenesis leading to such a ligation state in a distorted ferric heme would likely afford a spin state close to the pure mid-spin state ($S = 3/2$) of the type described in this paper, with characteristic spectral features similar to those reported above for the ethanol-ligated ferric tetramethylchiroporphyrin species.

Conclusion

We have demonstrated that it is possible to tune both the equatorial and the axial ligand fields of a ferric porphyrin to achieve a very strong tetragonal distortion around the iron center. Whereas a weak axial field, or a small porphyrin hole alone, usually leads to a moderate tetragonal distortion of the iron(III) complex and to a consequent mixed-spin state ($S = 3/2$, $5/2$), the combination of both effects in the [(TMCP)Fe^{III}(C_2H_5OH)$_2$]$^+$ and [(TMCP)Fe^{III}(C_2H_5OH)(H_2O)]$^+$ species results in a ground state which is a mid-spin state ($S = 3/2$), or very close to a mid-spin state at least. The biological relevance of these alcohol-ligated species is an open question, due to the rare occurrence of axial alcohol ligation in wild-type cytochromes. However, in addition to being exceptional magnetochemical curiosities, these species define the spectral signatures of a potential Tyr(OH)/Tyr(OH) or Tyr(OH)/H_2O ligation state that could be obtained by site-directed mutagenesis of a hemoprotein.

This investigation has also revealed a genuine case of bond-stretch isomerism,[52] in which hydrogen bonding from an aqua ligand of iron(III) to an interstitial ethanol or water molecule results in a significant contraction of the Fe−O(aqua) bond, and in an elongation of the *trans* Fe−O(ethanol) bond, relative to the same complex with an unperturbed aqua ligand. This hydrogen-bond-assisted modulation of axial ligation may have important implications in the control of hemoprotein structure and function.

Acknowledgment. This work was supported by the Centre National de la Recherche Scientifique (Grant URA 1194 to J.C.M.), the NIH (Grants GM-38401 and RR-06709 to W.R.S.), and the State Committee for Scientific Research KBN (Grant 2 2651 92 03 to L.L.G.).

Supporting Information Available: An X-ray crystallographic file (CIF). This material is available free of charge via the Internet at http://pubs.acs.org.

IC000150A

---

(46) Cys(42)Ser rubredoxin mutant: Xiao, Z.; Lavery, M. J.; Ayhan, M.; Scrofani, S. D. B.; Wilce, M. C. J.; Guss, J. M.; Tregloan, P. A.; George, G. N.; Wedd, A. G. *J. Am. Chem. Soc.* **1998**, *120*, 4135−4150.

(47) Cytochrome P-450 LM2: Jänig, G. R.; Makower, A.; Rabe, H.; Bernhardt, R.; Ruckpaul, K. *Biochim. Biophys. Acta* **1984**, *787*, 8−18.

(48) Cytochrome *f*: Martinez, S. E.; Huang, D.; Szczepaniak, A.; Cramer, W. A.; Smith, J. L. *Structure* **1994**, *2*, 95−105.

(49) Cytochrome *f*: Gao, F.; Qin, H.; Knaff, D. B.; Zhang, L.; Yu, L.; Yu, C. A.; Gray, K. A.; Daldal, F.; Ondrias, M. R. *Biochim. Biophys. Acta* **1999**, *1430*, 203−213.

(50) His(E7)Tyr Mb and His(F8)Tyr Mb: Egeberg, K. D.; Springer, B. A.; Martinis, S. A.; Sligar, S. G.; Morikis, D.; Champion, P. M. *Biochemistry* **1990**, *29*, 9783−9791.

(51) Heme d_1 of cytochrome cd_1: Cheesman, M. R.; Ferguson, S. J.; Moir, J. W. B.; Richardson, D. J.; Zumft, W. G.; Thomson, A. J. *Biochemistry* **1997**, *36*, 16267−16276.

(52) Parkin, G.; Hoffmann, R. H. *Angew. Chem., Int. Ed. Engl.* **1994**, *33*, 1462 and references therein.